Pivotal Role of Interdigitation in Interleaflet Interactions: Implications from Molecular Dynamics Simulations

Sangjae Seo [a, b], *Michio Murata* [c], *Wataru Shinoda* [a,*]

[a] Department of Materials Chemistry, Nagoya University, Nagoya, Japan

[b] Korean Institute of Science and Technology Information, Republic of Korea

[c] Graduate School of Science, Osaka University, Toyonaka, Osaka, Japan

*Corresponding Author: w.shinoda@chembio.nagoya-u.ac.jp

ABSTRACT

The asymmetric lipid composition in plasma membranes within the inner leaflet is not typically suitable for domain formation. Thus, elucidation of the likelihood of the formation or stability of a raft-like domain in the inner leaflet is necessitated. Herein, we investigated the phase behavior of asymmetric membranes using coarse-grained molecular dynamics simulations. The lipid leaflet comprising dioleoylphosphatidylcholine (DOPC) and cholesterol (Chol) does not typically show well-developed domains in symmetric bilayer membranes; however, it does separate into liquid ordered (L_o) and liquid disordered (L_d) phases when the opposing leaflet containing sphingomyelin (SM), DOPC, and Chol demonstrate domain formation. We determine that interdigitated acyl chains modulated the partitioning of Chol in the opposing leaflet, resulting in phase separation. Similarly, the acyl chain length of SM within the opposing leaflet affected the phase behavior of the leaflet. Our results reveal the crucial role of interdigitation in determining the phase status in asymmetric membranes.

TOC GRAPHICS

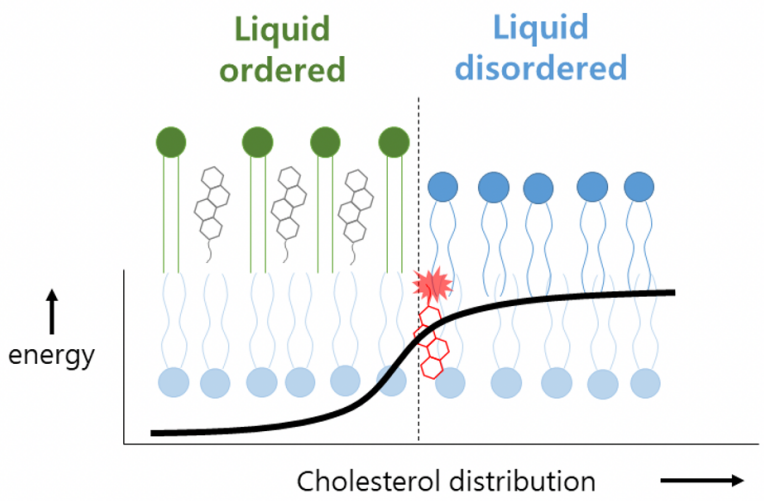

KEYWORDS: Lipid raft, asymmetric membrane, interdigitation, inter-leaflet coupling. coarse-grained molecular dynamics simulation.

Abbreviations: DPPC, 1,2-dipalmitoyl-sn-glycero-3-phophocholine; DOPC, 1,2-dioleoyl-sn-glycero-3-phosphocholine; PSM, N-palmitoyl-d-erythro-sphingosylphosphorylcholine; ASM, N-arachidoyl-d-erythro-sphingosylphosphorylcholine; LSM, N-lignoceroyl-d-erythro-sphingosylphosphorylcholine; Chol, cholesterol;

Heterogeneous molecular distribution in the plasma membrane has gained significant attention due to its biological importance[1–3], especially since the lipid raft model proposed lateral heterogeneity of the plasma membrane. Favorable interactions between cholesterol (Chol) and saturated lipids were shown to induce phase separation of the lipid membrane into liquid- ordered (L_o) and disordered (L_d) phases[4–6]. Since lipid rafts play a crucial role in biological functions, such as protein sorting, signal transduction, and viral fusion[7–13], it is of great importance to understand the structure and characteristics of lipid rafts. Since the first optical observation of lipid rafts in a model vesicle[14], subsequent studies have revealed the physicochemical properties of lipid rafts[15–19].

Interleaflet interaction has been recognized as an important consideration in understanding the phase separation of the lipid membrane. Many studies have shown that lipid rafts in each leaflet do not exist independently; instead, there is a strong coupling of L_o domains between the leaflets. It was estimated[20–22] that the inter-leaflet coupling strength is in the range of 0.01–1 k_BT/nm^2. In addition, theoretical studies suggest that the strong coupling between leaflets results in the domain registration (phase symmetry)[23]. Owing to its complexity, there is currently no consensus on the mechanism of the interleaflet coupling, although several hypotheses, such as electrostatic coupling, interdigitation, curvature, and transmembrane proteins, have been proposed[24,25].

Since the cellular membrane consists of asymmetric lipids, the role of the interleaflet interaction in determining phase behavior becomes more important. In order to optically detect lipid rafts, model vesicles were employed; these are typically composed of phosphatidylcholines (PC), sphingomyelins (SM), and Chols, which are the major lipids found in the outer leaflet of the plasma membrane[4,14]. However, domain formation was not detected in lipid membranes with the lipid composition of the inner leaflet[26,27]. There have been experimental observations demonstrating that

L_o or Chol-enriched domains in one leaflet induces domain formation in the opposing leaflet[27–31]. Similarly, MD simulations have also shown preferential ordering of lipid tails owing to domain formation in the opposing leaflet[32–34]. The results suggest that either curvature or acyl chain interdigitation may have a role in the ordering of acyl tails. Nevertheless, even though Chol enrichment is essential to promote L_o phase formation at physiological temperature, there is currently no clear explanation for the localization of Chols in the L_o domains of the opposing leaflet due to the inter-leaflet interaction in asymmetric membrane.

In this work, we investigated domain formation by interleaflet coupling in asymmetric membranes using coarse-grained (CG) MD simulations. We exploited the SPICA force field[35–40], which was recently developed to accurately predict the phase behavior of lipid membranes containing Chol and SM. Unlike previous MD studies that were concerned with acyl chain ordering, we have focused our study on Chol partitioning in the regions facing to the L_o and L_d domains. In addition, the effects of the acyl chain length of SMs on domain formation across leaflets were studied.

To mimic the conditions in which the inner leaflet cannot form domains alone, we prepared the asymmetric membrane PSM:DOPC:Chol(up)/DOPC:Chol(low) in roughly 1:1:1 ratio (See Table S1 for details). In this paper, "up" and "low" in the parentheses indicate the upper and lower leaflet compositions, respectively. In our previous work[35], the symmetric membrane SM:DOPC:Chol in 1:1:1 ratio was found to separate into L_o and L_d phases. In the absence of saturated lipids, however, the lipids in the binary-mixed membrane DOPC:Chols (< 40% Chol) were randomly distributed, showing no clustering, regardless of the Chol content. However, in the case of the asymmetric membrane PSM:DOPC:Chol(up)/DOPC:Chol(low), the phase behavior of the lower leaflet was remarkably different, as shown in Fig. 1.

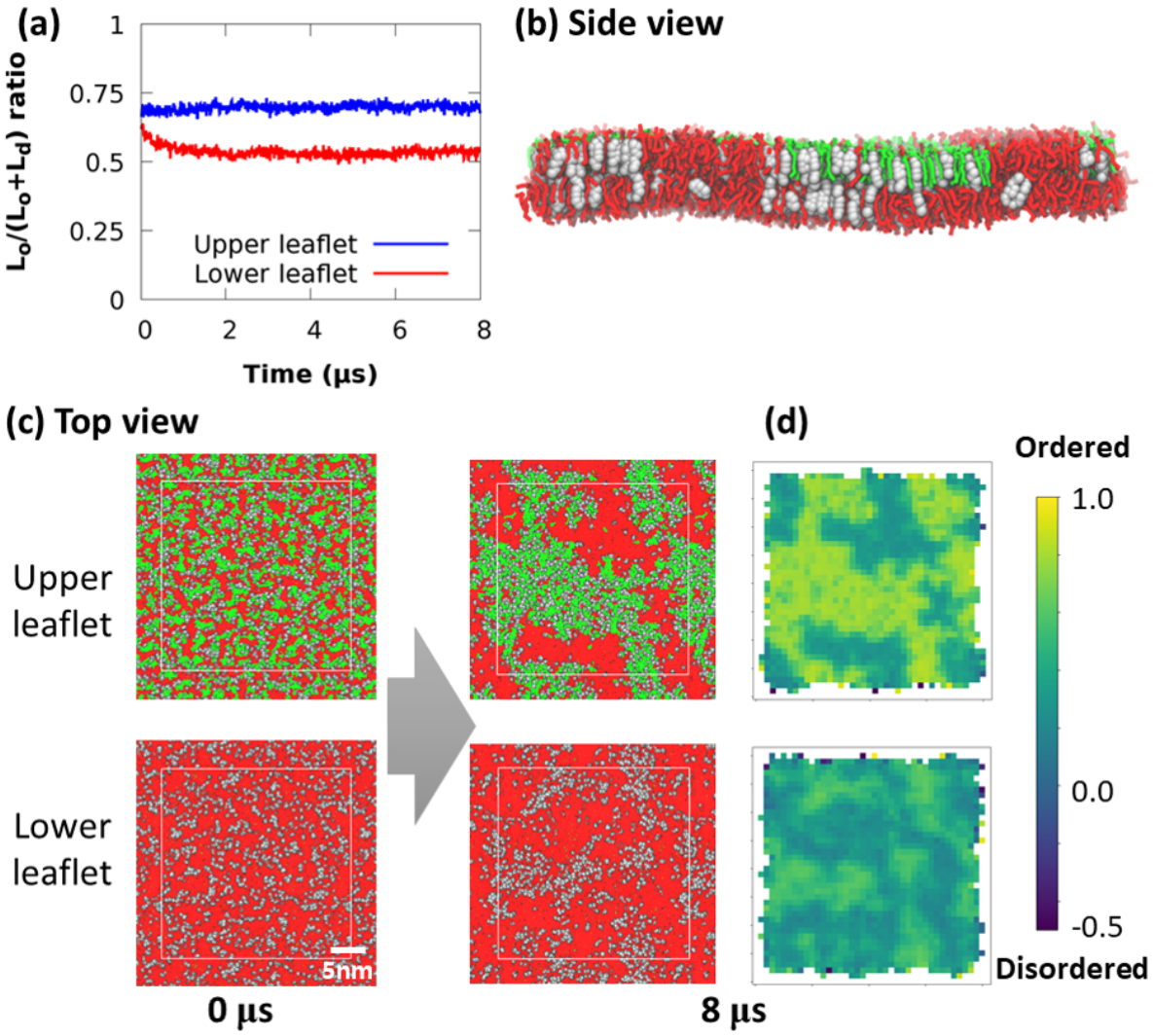

Figure 1. Phase behavior of PSM:DOPC:Chol/ DOPC:Chol. (a) Time evolution of the L_o ratio during the simulation. (b) The side view of the membrane at 8 μs. (c) The top view of the snapshots at the initial (0 μs) and final (8 μs) states of the MD simulation. Color code is as follows: Red: DOPC, Green: PSM, and Silver: Cholesterol. (d) Averaged order parameter distributions over the last 100 ns trajectory in the 8 μs MD run.

Figure 1 depicts the L_o / (L_o + L_d) ratio in each leaflet during the course of the MD simulation, the final snapshot of the membrane system, and the order parameter distribution in each leaflet calculated over the last 100 ns trajectory of the 8 μs MD run. In order to distinguish L_o and L_d domains, we calculated the CG order parameter, which measures the degrees of order of the tail chain, in a manner similar to the calculation of the deuterium NMR order parameter (see SI for details). We regard the lipid to be in the L_o state if the CG order parameter is larger than 0.7 and 0.35 for SM and DOPC, respectively. The criteria to distinguish L_o and L_d domains were determined based on the average CG order parameters in the binary systems containing 40% Chol. The proportion of L_o domains maintained larger than 50% in both leaflets (Fig 1(a)), clearly demonstrating phase separation. In addition, the locations of the high order parameter coincide with that of the high Chol distribution (Fig 1(b, c, d)). This clearly shows preferential ordering of the lipid tail owing to Chol enrichment. The inhomogeneous distributions of Chol and the order parameter also indicate phase separation of the membrane. As expected, we observed a clear phase separation of the upper leaflet into the L_o and L_d domains. Interestingly, although the lower leaflet only contains DOPC and Chol, heterogeneous distribution of Chol and the order parameter across the leaflets indicate a similar phase separation in the lower leaflet. In addition, interleaflet coupling of the L_o domains in the upper and lower leaflets was evident. To quantify the registration of the L_o domains, we calculated the ratio between the registered and anti-registered domains. The registration ratio of the L_o domains between the upper and lower leaflets rapidly increased in the early stage of simulation and saturated above 50% (Fig. S1). Thus, in the PSM:DOPC:Chol(up)/ DOPC:Chol(low) membrane, domain formation in the upper leaflet was found to induce domain formation in the lower leaflet.

Since it is natural to consider that interleaflet coupling should correlate with the acyl chain length, it has been speculated that the long-chain SM may have an important role in interleaflet communication[41]. To investigate how the acyl chain length affects the domain formation, we performed comparative CG-MD simulations on the membranes of LSM:DOPC:Chol(up)/ DPPC:DOPC:Chol(low) in 1:1:1 ratio and PSM:DOPC:Chol(up)/DPPC:DOPC:Chol(low). In these cases, we expect that both leaflets show a phase separation in their symmetric bilayers. Thus, the system is useful to examine whether the long acyl chained SM promotes or hinders domain formation in the opposing leaflet.

Figure 2 illustrates the phase behavior of the membranes after 8 μs of CG-MD starting from the randomly mixed asymmetric membranes. As expected, in all cases, the upper leaflets consisting of SM:DOPC:Chol showed phase separation into L_o and L_d phases. We detected domains enriched with Chol, corresponding to regions with the higher order parameter. Interestingly, an obvious difference in the interleaflet coupling was detected between the two membranes containing PSM and LSM. In the case of the PSM membrane, domain formation in the lower leaflet was clearly observed. The L_o domains in both leaflets were registered (phase symmetry). In the case of the LSM membrane, the lower leaflet showed a smaller L_o domain, compared to the PSM membrane. In addition, the L_o domains are not in registry; instead, the formation of anti-registered (phase asymmetry) domains was observed. The registration ratio clearly shows the different phase behavior between PSM and LSM (Fig. 2(c)).

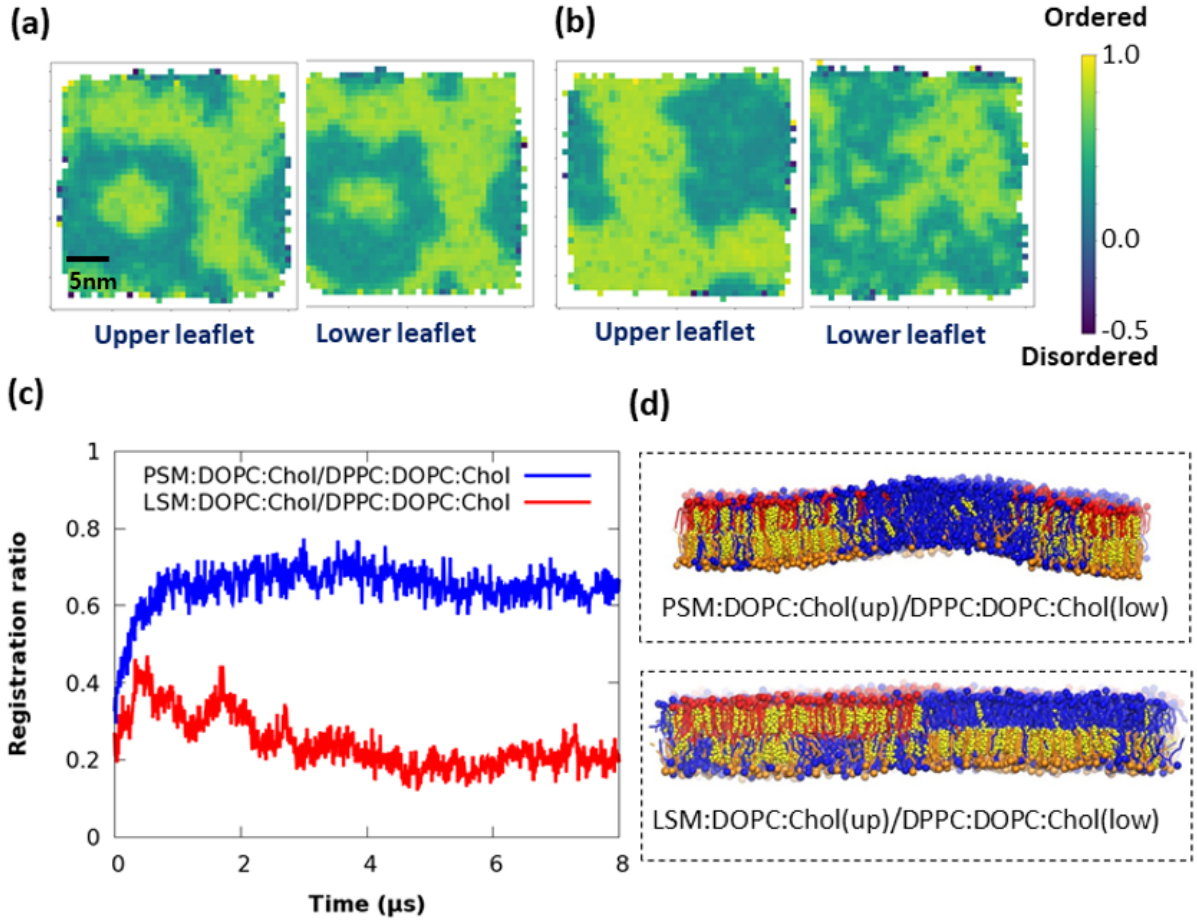

Figure 2. Phase behavior of PSM:DOPC:Chol(up)/DPPC:DOPC:Chol(low) and LSM:DOPC:Chol(up)/DPPC:DOPC:Chol(low) after 8 μs simulation. Averaged order parameter distributions of systems of (a) PSM:DOPC:Chol(up)/DPPC:DOPC:Chol(low) and (b) LSM:DOPC:Chol(up)/DPPC:DOPC:Chol(low) over 100 ns at 8 μs. (c) Order parameter registration ratio. (d) Snapshot of the side view at 8 μs. Color code is as follows: Red: PSM, Blue: DOPC, Orange: DPPC, and Yellow: Cholesterol.

As seen in Fig. 2(c), in the membrane containing PSM, the registration ratio increased up to ~0.7. However, the registration ratio of the membrane containing LSM started decreasing at approximately 0.3 μs, and finally only a 0.2 fraction of L_o domains are registered. This result

indicates that the L_o domain containing LSM in the upper leaflet expels the L_o domain and even prohibits the formation of large domains in the lower leaflet.

In our CG MD simulations on the mixture systems, we found that the partitioning of Chol is highly affected by the composition of the opposing leaflet. As the tail length of SM (i.e., PSM and LSM) was observed to alter the phase status in the opposing leaflet, we further investigated the partitioning of Chol depending on the acyl chain compositions in the opposing leaflet. For this purpose, because it is difficult to systematically quantify the preference of Chol in the mixture systems, we prepared simple systems, which contain only DOPC in the upper leaflet and various compositions in the lower leaflet: DOPC, PSM(C16:0):Chol, ASM(C20:0):Chol, and LSM(C24:0):Chol. In addition, we prepared the DOPC+Chol(up)/PSM+Chol(low) system to further observe the effect of interdigitation. We measured the transfer free energy (TFE) of Chol molecule from membrane to water to quantitatively measure the preference of Chol partitioning. TFE was calculated by transferring one Chol molecule embedded in the upper leaflet (DOPC only) from its stable position to the bulk water region. The required free energy for the transfer was calculated using the adaptive biasing force (ABF; for the details refer to Refs. [42] and [43]) method. In order to avoid the energetic contribution resulting from area mismatch, we verified that the area of the two leaflets agreed with each other, and confirmed that the tilt angle distribution and CG order parameter of the DOPC leaflet did not change significantly.

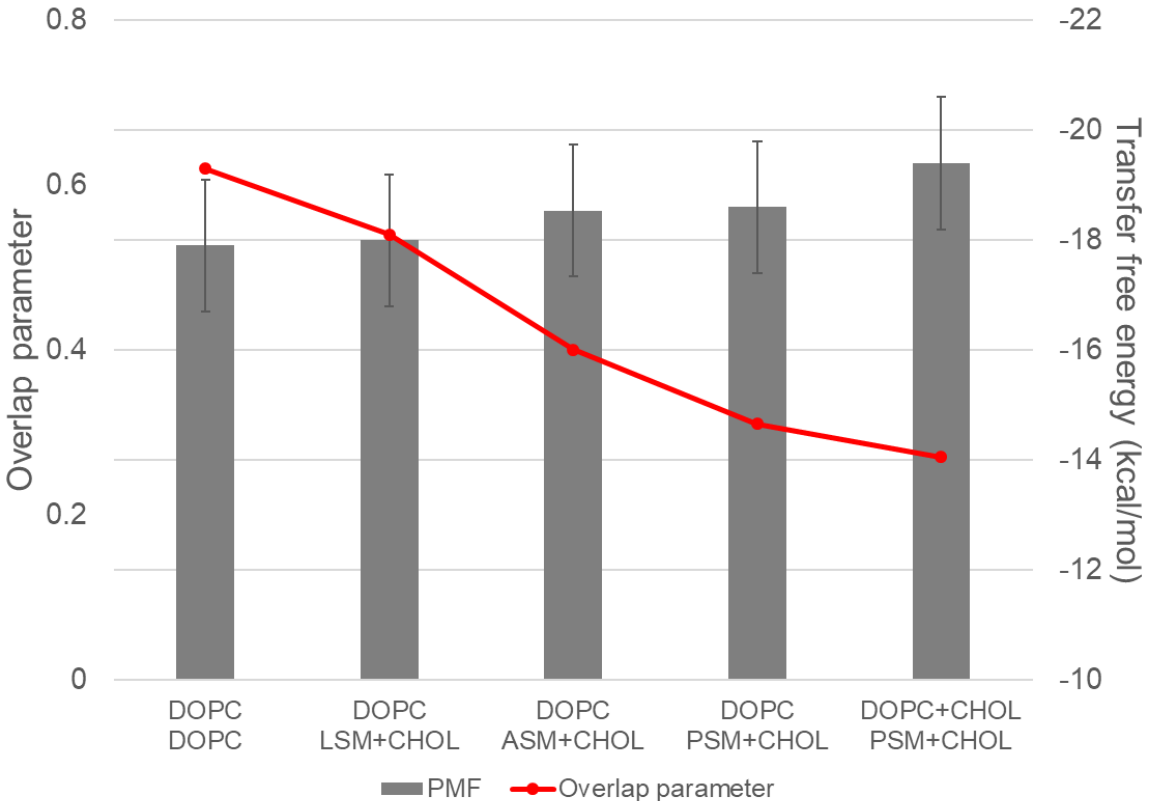

Figure 3. Transfer free energy of Chol and overlap parameter in simple systems. The top and bottom rows of the x-axis tick labels denote the lipid components in the upper and lower leaflets, respectively.

Figure 3 depicts the TFE of Chol with respect to the opposing leaflet compositions. Despite the relatively large statistical error of the TFE, one can clearly observe the differences between the systems. The DOPC(up)/DOPC(low) membrane shows the smallest energy gain, while the DOPC+Chol(up)/PSM+Chol(low) shows the largest energy gain, i.e., when Chol was added to the DOPC layer. By varying the type of SM, we found that the free energy gain of Chol is affected by the acyl chain length in the opposing leaflet. As the acyl chain length of SM increased, less free energy gain was observed. Since longer acyl chains readily penetrate deeper in the opposing leaflet, we speculated that acyl chain interdigitation and Chol partitioning are strongly related. We

quantified the degrees of interdigitation, namely the overlap parameter (see SI), and compared it with TFE. Higher value of the overlap parameter indicates the deeper penetration (stronger interdigitation) of acyl chains from opposing leaflet. In Fig. 3, the red line shows the overlap parameter in each system. Interestingly, a clear correlation was observed between the level of interdigitation and TFE. The DOPC(up)/DOPC(low) membrane shows the largest overlap parameter and the smallest energy gain, while the DOPC+Chol(up)/PSM+Chol(low) membrane shows the smallest overlap parameter and the largest free energy gain. In addition, longer tails of SMs increased the TFE of Chol in the opposing leaflet. The results indicate that the partitioning of Chol is unfavorable in the highly interdigitated region.

Indeed, we found a strong correlation between the location of the L_o domains and interdigitation in the mixture systems. To compare with the simple systems, we calculated the free energy gain of Chol between the Chol-depleted region (representing L_d) and the Chol-enriched region (representing L_o) from the distribution of Chol (see SI). The free energy gain owing to the phase status in the opposing leaflet between the regions facing L_o and L_d in the mixture system shows a similar value to the simple systems, which is -2.0 k_BT (c.a. -1.2 kcal/mol). We also calculated the average overlap parameters in each pixel on the mixture membrane surface to compare the phase status and interdigitation. In the case of the membrane containing PSM, it was found that the highly interdigitated regions (i.e., where the higher overlap parameters are found) clearly correspond to the L_d domains (Fig. 4(a, b)). Accordingly, the L_o domains show much smaller overlap parameters than the L_d domains. In contrast, in the membrane containing LSM, the overlap distribution does not show a clear correlation with the domain distribution (Fig 4(c)).

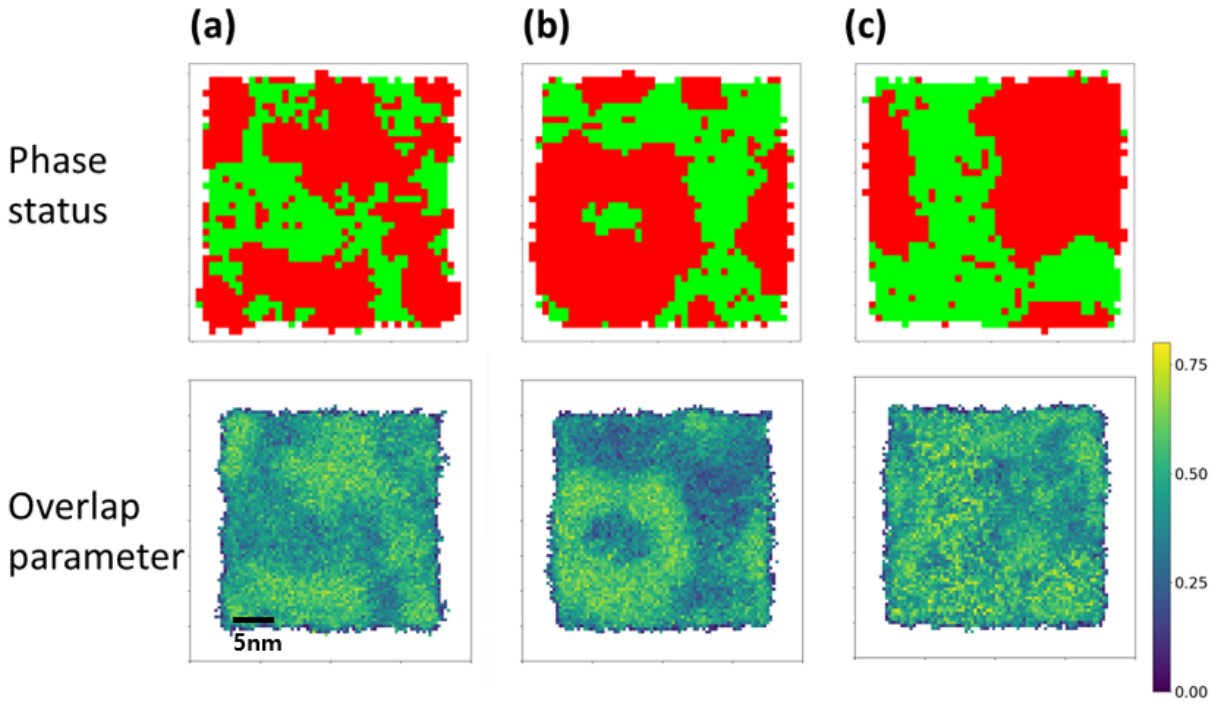

Figure 4. Interdigitation of the acyl chain at 8 μs. (a) PSM:DOPC:Chol(up)/DOPC:Chol(low), (b) PSM:DOPC:Chol(up)/DPPC:DOPC:Chol(low), and (c) LSM:DOPC:Chol(up)/DPPC:DOPC:Chol(low). Upper panels: phase status of the upper leaflet of each system. Green and red indicate the L_o and L_d phases, respectively. Lower panels: overlap parameter distribution.

Because the enrichment of Chol gives rise to the condensation of the acyl tail, which leads to the formation of L_o domains, it is of great importance to understand how Chol partitioning is promoted. Our MD simulation results suggest that the interdigitation of acyl chains is one of the key factors that drives Chol partitioning. The MD simulation results of the mixture system showed that the leaflet could be phase separated into L_o and L_d phases, even in the absence of saturated lipids. Free energy calculation indicates that the penetration of the acyl tail from the opposing leaflet discourages Chol partitioning. Accordingly, Chol tends to move to the region of the opposing L_o phase when it is free from the long SM, resulting in the phase separation of the leaflet even without

saturated lipids. Conversely, the long acyl chain in the L_o domain inhibits L_o domain formation in the opposing leaflet. Therefore, in relation to the cellular membrane, our results suggest that the L_o domains in the inner leaflet, which lacks SM lipids, can be induced by the L_o domain in the outer leaflet, regardless of the presence of saturated lipids.

Obviously, the phases in the membrane is not determined by one factor. In particular, interleaflet coupling is affected by various factors, such as interdigitation of the acyl chain, membrane curvature, hydrophobic mismatch between domains, and the presence of transmembrane proteins. Amongst these, we showed that the interdigitation itself is capable of controlling the lipid domains. Moreover, experimental evidence demonstrated that the interdigitation of long acyl chains directly affects cellular activities[44–46]. These experiments inform us of the paramount importance of interdigitation. In this regard, this study offers profound insight into the molecular mechanism of interleaflet interactions in the cellular membrane.

EXPERIMENTAL METHODS

We prepared asymmetric membranes using CHARMM-GUI[47] and PACKMOL[48]. Initial configurations of small patches were constructed by CHARMM-GUI, and the unit patches were duplicated by PACKMOL to enlarge the system size. Table S1 lists the systems we conducted in this study. All simulations were run using LAMMPS[49] with the SPICA force field[35–40]. In all simulations, the temperature was maintained at 298 K using the Nosé-Hover thermostat[50,51]. The semi-isotropic pressure control was applied at 1 atm using the Parrinello-Rahman barostat[52,53] with a response time of 5 ps. The cut-off scheme was used for the LJ-type interaction (r_{cut}=1.5 nm), while the particle-particle particle-mesh method[54] was used to calculate long-range electrostatic interactions. A time step of 10 fs was used in all MD simulations.

ASSOCIATED CONTENT

Supporting Information.

The following files are available free of charge.

Further details regarding the system preparation, analyses protocol, summary of system and additional plots (registration ratio, number of cholesterol, membrane area, terminal bead distribution, cholesterol distribution). (PDF)

AUTHOR INFORMATION

Address: Department of Materials Chemistry, Nagoya University, Nagoya, Japan

E-mail: w.shinoda@chembio.nagoya-u.ac.jp

Phone: +81-52-789-5288

ACKNOWLEDGMENTS

This research was supported by JSPS KAKENHI Grant No. 16H06315 and also by MEXT as "Program for Promoting Researches on the Supercomputer Fugaku" (Biomolecular dynamics and function in a living cell using atomistic and coarse-grained simulations) and "Priority Issue on Post-K computer" (Building Innovative Drug Discovery Infrastructure Through Functional Control of Biomolecular Systems). Calculations were performed at the facilities of the Research Center for Computational Science, Okazaki, the Institute for Solid State Physics, the University of

Tokyo, and in part on the K-computer hosted at the RIKEN Advanced Institute for Computational Science (Proposal Nos. hp180191 and hp190171).

REFERENCES

(1) Simons, K.; Ikonen, E. Functional Rafts in Cell Membranes. *Nature* **1997**, *387*, 569–572.

(2) Brown, D. A.; London, E. Functions of Lipid Rafts in Biological Membranes. *Annu. Rev. Cell Dev. Biol.* **1998**, *14*, 111–136.

(3) Simons, K.; Vaz, W. L. C. Model Systems, Lipid Rafts, and Cell Membranes. *Annu. Rev. Biophys. Biomol. Struct.* **2004**, *33*, 269–295.

(4) Veatch, S. L.; Keller, S. L. Organization in Lipid Membranes Containing Cholesterol. *Phys. Rev. Lett.* **2002**, *89*, 268101.

(5) Munro, S. Lipid Rafts: Elusive or Illusive? *Cell* **2003**, *115*, 377–388.

(6) Pike, L. J. Rafts Defined: A Report on the Keystone Symposium on Lipid Rafts and Cell Function. *J. Lipid Res.* **2006**, *47*, 1597–1598.

(7) Simons, K.; Toomre, D. Lipid Rafts and Signal Transduction. *Nat. Rev. Mol. Cell Biol.* **2000**, *1*, 31–39.

(8) Slimane, T. A.; Trugnan, G.; van IJzendoorn, S. C. D.; Hoekstra, D. Raft-Mediated Trafficking of Apical Resident Proteins Occurs in Both Direct and Transcytotic Pathways

in Polarized Hepatic Cells: Role of Distinct Lipid Microdomains. *Mol. Biol. Cell* **2003**, *14*, 611–624.

(9) de Gassart, A. Lipid Raft-Associated Protein Sorting in Exosomes. *Blood* **2003**, *102*, 4336–4344.

(10) Takeda, M.; Leser, G. P.; Russell, C. J.; Lamb, R. A. Influenza Virus Hemagglutinin Concentrates in Lipid Raft Microdomains for Efficient Viral Fusion. *Proc. Natl. Acad. Sci.* **2003**, *100*, 14610–14617.

(11) Helms, J. B.; Zurzolo, C. Lipids as Targeting Signals: Lipid Rafts and Intracellular Trafficking. *Traffic* **2004**, *5*, 247–254.

(12) Schafer, L. V.; de Jong, D. H.; Holt, A.; Rzepiela, A. J.; de Vries, A. H.; Poolman, B.; Killian, J. A.; Marrink, S. J. Lipid Packing Drives the Segregation of Transmembrane Helices into Disordered Lipid Domains in Model Membranes. *Proc. Natl. Acad. Sci.* **2011**, *108*, 1343–1348.

(13) Yang, S.-T.; Kiessling, V.; Simmons, J. A.; White, J. M.; Tamm, L. K. HIV Gp41–Mediated Membrane Fusion Occurs at Edges of Cholesterol-Rich Lipid Domains. *Nat. Chem. Biol.* **2015**, *11*, 424–431.

(14) Veatch, S. L.; Keller, S. L. Separation of Liquid Phases in Giant Vesicles of Ternary Mixtures of Phospholipids and Cholesterol. *Biophys. J.* **2003**, *85*, 3074–3083.

(15) de Almeida, R. F. M.; Loura, L. M. S.; Fedorov, A.; Prieto, M. Lipid Rafts Have Different Sizes Depending on Membrane Composition: A Time-Resolved Fluorescence Resonance Energy Transfer Study. *J. Mol. Biol.* **2005**, *346*, 1109–1120.

(16) Veatch, S. L.; Polozov, I. V.; Gawrisch, K.; Keller, S. L. Liquid Domains in Vesicles Investigated by NMR and Fluorescence Microscopy. *Biophys. J.* **2004**, *86*, 2910–2922.

(17) Levental, I.; Grzybek, M.; Simons, K. Raft Domains of Variable Properties and Compositions in Plasma Membrane Vesicles. *Proc. Natl. Acad. Sci.* **2011**, *108*, 11411–11416.

(18) Risselada, H. J.; Marrink, S. J. The Molecular Face of Lipid Rafts in Model Membranes. *Proc. Natl. Acad. Sci.* **2008**, *105*, 17367–17372.

(19) Sezgin, E.; Levental, I.; Mayor, S.; Eggeling, C. The Mystery of Membrane Organization: Composition, Regulation and Roles of Lipid Rafts. *Nat. Rev. Mol. Cell Biol.* **2017**, *18*, 361–374.

(20) Collins, M. D. Interleaflet Coupling Mechanisms in Bilayers of Lipids and Cholesterol. *Biophys. J.* **2008**, *94*, L32–L34.

(21) Putzel, G. G.; Uline, M. J.; Szleifer, I.; Schick, M. Interleaflet Coupling and Domain Registry in Phase-Separated Lipid Bilayers. *Biophys. J.* **2011**, *100*, 996–1004.

(22) Haataja, M. P. Lipid Domain Co-Localization Induced by Membrane Undulations. *Biophys. J.* **2017**, *112*, 655–662.

(23) Fujimoto, T.; Parmryd, I. Interleaflet Coupling, Pinning, and Leaflet Asymmetry—Major Players in Plasma Membrane Nanodomain Formation. *Front. Cell Dev. Biol.* **2017**, *4*, 155.

(24) May, S. Trans-Monolayer Coupling of Fluid Domains in Lipid Bilayers. *Soft Matter* **2009**, *5*, 3148-3156.

(25) Eicher, B.; Marquardt, D.; Heberle, F. A.; Letofsky-Papst, I.; Rechberger, G. N.; Appavou, M.-S.; Katsaras, J.; Pabst, G. Intrinsic Curvature-Mediated Transbilayer Coupling in Asymmetric Lipid Vesicles. *Biophysj* **2018**, *114*, 146–157.

(26) Wang, T.-Y.; Silvius, J. R. Cholesterol Does Not Induce Segregation of Liquid-Ordered Domains in Bilayers Modeling the Inner Leaflet of the Plasma Membrane. *Biophys. J.* **2001**, *81*, 2762–2773.

(27) Collins, M. D.; Keller, S. L. Tuning Lipid Mixtures to Induce or Suppress Domain Formation across Leaflets of Unsupported Asymmetric Bilayers. *Proc. Natl. Acad. Sci.* **2008**, *105*, 124–128.

(28) Cheng, H.-T.; London, E. Preparation and Properties of Asymmetric Large Unilamellar Vesicles: Interleaflet Coupling in Asymmetric Vesicles Is Dependent on Temperature but Not Curvature. *Biophys. J.* **2011**, *100*, 2671–2678.

(29) Chiantia, S.; London, E. Acyl Chain Length and Saturation Modulate Interleaflet Coupling in Asymmetric Bilayers: Effects on Dynamics and Structural Order. *Biophys. J.* **2012**, *103*, 2311–2319, DOI:10.1016/j.bpj.2012.10.033.

(30) Lin, Q.; London, E. Ordered Raft Domains Induced by Outer Leaflet Sphingomyelin in Cholesterol-Rich Asymmetric Vesicles. *Biophys. J.* **2015**, *108*, 2212–2222.

(31) Wang, Q.; London, E. Lipid Structure and Composition Control Consequences of Interleaflet Coupling in Asymmetric Vesicles. *Biophys. J.* **2018**, *115*, 664–678.

(32) Perlmutter, J. D.; Sachs, J. N. Interleaflet Interaction and Asymmetry in Phase Separated Lipid Bilayers: Molecular Dynamics Simulations. *J. Am. Chem. Soc.* **2011**, *133*, 6563–6577.

(33) Róg, T.; Orłowski, A.; Llorente, A.; Skotland, T.; Sylvänne, T.; Kauhanen, D.; Ekroos, K.; Sandvig, K.; Vattulainen, I. Interdigitation of Long-Chain Sphingomyelin Induces Coupling of Membrane Leaflets in a Cholesterol Dependent Manner. *Biochim. Biophys. Acta - Biomembr.* **2016**, *1858*, 281–288.

(34) Manna, M.; Javanainen, M.; Monne, H. M.-S.; Gabius, H.-J.; Rog, T.; Vattulainen, I. Long-Chain GM1 Gangliosides Alter Transmembrane Domain Registration through Interdigitation. *Biochim. Biophys. Acta - Biomembr.* **2017**, *1859*, 870–878.

(35) Seo, S.; Shinoda, W. SPICA Force Field for Lipid Membranes: Domain Formation Induced by Cholesterol. *J. Chem. Theory Comput.* **2019**, *15*, 762-774.

(36) Shinoda, W.; DeVane, R.; Klein, M. L. Multi-property fitting and parameterization of a coarse grained model for aqueous surfactants. *Mol. Simul.* **2007**, *33*, 27-36.

(37) Shinoda, W.; DeVane, R.; Klein, M. L. Coarse-grained molecular modeling of non-ionic surfactant self-assembly. *Soft Matter*, **2008**, *4*, 2454-2462.

(38) Shinoda, W.; DeVane, R.; Klein, M. L. Zwitterionic lipid assemblies: molecular dynamics studies of monolayers, bilayers, and vesicles using a new coarse grain force field. *J. Phys. Chem. B*, **2010**, *114*, 6836-6849.

(39) Shinoda, W.; DeVane, R.; Klein, M. L. Coarse-grained force field for ionic surfactants. *Soft Matter*, **2011**, *7*, 6178-6186.

(40) Shinoda, W.; DeVane, R.; Klein, M. L. Computer simulation studies of self-assembling macromolecules. *Curr. Opin. Struct. Biol.* **2012**, *22*, 175-186.

(41) Róg, T.; Orłowski, A.; Llorente, A.; Skotland, T.; Sylvänne, T.; Kauhanen, D.; Ekroos, K.; Sandvig, K.; Vattulainen, I. Interdigitation of Long-Chain Sphingomyelin Induces Coupling of Membrane Leaflets in a Cholesterol Dependent Manner. *Biochim. Biophys. Acta - Biomembr.* **2016**, *1858*, 281–288.

(42) Darve, E.; Pohorille, A. Calculating Free Energies Using Average Force. *J. Chem. Phys.*. **2001**, *115,* 9169–9183.

(43) Comer, J.; Gumbart, J. C.; Hénin, J.; Lelièvre, T.; Pohorille, A.; Chipot, C. The Adaptive Biasing Force Method: Everything You Always Wanted To Know but Were Afraid To Ask. *J. Phys. Chem. B.* **2015**, *119*, 1129–1151.

(44) Sassa, T.; Suto, S.; Okayasu, Y.; Kihara, A. A Shift in Sphingolipid Composition from C24 to C16 Increases Susceptibility to Apoptosis in HeLa Cells. *Biochim. Biophys. Acta* **2012**, *1821*, 1031–1037.

(45) Maté, S.; Busto, J. V.; García-Arribas, A. B.; Sot, J.; Vazquez, R.; Herlax, V.; Wolf, C.; Bakás, L.; Goñi, F. M. N-Nervonoylsphingomyelin (C24:1) Prevents Lateral Heterogeneity in Cholesterol-Containing Membranes. *Biophys. J.* **2014**, *106*, 2606–2616.

(46) Lazzarini, A.; Macchiarulo, A.; Floridi, A.; Coletti, A.; Cataldi, S.; Codini, M.; Lazzarini, R.; Bartoccini, E.; Cascianelli, G.; Ambesi-Impiombato, F. S.; et al. Very-Long-Chain Fatty Acid Sphingomyelin in Nuclear Lipid Microdomains of Hepatocytes and Hepatoma

Cells: Can the Exchange from C24:0 to C16:0 Affect Signal Proteins and Vitamin D Receptor? *Mol. Biol. Cell* **2015**, *26*, 2418–2425.

(47) Lee, J.; Cheng, X.; Swails, J. M.; Yeom, M. S.; Eastman, P. K.; Lemkul, J. A.; Wei, S.; Buckner, J.; Jeong, J. C.; Qi, Y.; et al. CHARMM-GUI Input Generator for NAMD, GROMACS, AMBER, OpenMM, and CHARMM/OpenMM Simulations Using the CHARMM36 Additive Force Field. *J. Chem. Theory Comput.* **2016**, *12*, 405–413.

(48) Martínez, L.; Andrade, R.; Birgin, E. G.; Martínez, J. M. PACKMOL: A Package for Building Initial Configurations for Molecular Dynamics Simulations. *J. Comput. Chem.* **2009**, *30*, 2157–2164.

(49) Plimpton, S. Fast Parallel Algorithms for Short-Range Molecular Dynamics. *J. Comput. Phys.* **1995**, *117*, 1–19.

(50) Nosé, S. A Unified Formulation of the Constant Temperature Molecular Dynamics Methods. *J. Chem. Phys.* **1984**, *81*, 511–519.

(51) Hoover, W. G. Canonical Dynamics: Equilibrium Phase-Space Distributions. *Phys. Rev. A* **1985**, *31*, 1695–1697.

(52) Parrinello, M.; Rahman, A. Crystal Structure and Pair Potentials: A Molecular-Dynamics Study. *Phys. Rev. Lett.* **1980**, *45*, 1196–1199.

(53) Parrinello, M.; Rahman, A. Polymorphic Transitions in Single Crystals: A New Molecular Dynamics Method. *J. Appl. Phys.* **1981**, *52*, 7182–7190.

(54) Hockney, R. W.; Eastwood, J. W. *Computer Simulation Using Particles*; Taylor & Francis, Inc.: Bristol, PA, USA, 1988.